ISSN 1560-8034, 1605-6582 (On-line), SPQEO, 2019. V. 22, N 4. P. 424-429.

Hetero- and low-dimensional structures

Numerical analysis of aluminum nanoparticle influence on the characteristics of a thin-film solar cell

A.B. Gnilenko[1,2], S.V. Plaksin[2]

[1]*Oles Honchar Dnipro National University, 72, Gagarin Ave., 49010 Dnipro, Ukraine*
[2]*Institute of Transport Systems and Technology, National Academy of Science of Ukraine, 5, Pisarzhevskogo str., 49056 Dnipro, Ukraine*
E-mail: svp@westa-inter.com

Abstract. The influence of parameters of an aluminum nanoparticle layer on the characteristics of a thin-film amorphous silicon solar cell has been studied using the computer simulation methods. A design with a regular arrangement of nanoparticles both on the front and back sides of the solar cell has been considered. The distribution of photogeneration rate in the amorphous silicon layer has been obtained for different values of the nanoparticle radius. The effects of nanoparticle radius and nanoparticle spacing on the electrical characteristics of a solar cell have been analyzed. It has been shown that, with optimal parameters of nanoparticles, it is possible to significantly increase the efficiency of solar cells.

Keywords: Silvaco TCAD, amorphous silicon, photogeneration rate, *I-V* characteristics, solar cell efficiency.

https://doi.org/10.15407/spqeo22.04.424
PACS 88.40.hj, jj

Manuscript received 04.07.19; revised version received 21.07.19; accepted for publication 29.10.19; published online 08.11.19.

1. Introduction

In the history of development of solar energetics, it is usual to emphasize three generations of solar cells. The first generation includes classic silicon solar cells with one *p-n* junction and a photoactive silicon layer thickness of about 200…300 μm. These solar cells demonstrate high efficiency values within the range 16…22% and still dominate the market of photovoltaic cells. In the second generation of solar cells, amorphous silicon (a-Si:H), cadmium telluride (CdTe) or a compound of copper, indium, gallium and selenium (CIGS) are used instead of crystalline silicon. Since the thickness of the photoactive layer for these semiconductor materials does not exceed 3-4 μm, solar power converters constructed on their base are defined as thin-film solar cells. Despite low efficiency, not exceeding 14%, thin-film solar cells have a lower cost per watt, lower efficiency losses in adverse conditions, as well as a simpler and more reliable low-budget manufacturing technology of solar modules. All this leads to a constant increase in the share of thin-film solar cells on the market, mainly due to the use of amorphous silicon solar cells. The third generation of solar cells [1] comprises a wide class of photoelectric converters created on the basis of new, non-standard technical and technological solutions. Although solar cells of third generation do not yet have their stable market share, they are rapidly developing and demonstrating high efficiency levels at low cost. These solar cells are mainly thin-film photoelectric converters using non-standard materials, namely: organic polymers, perovskite, graphene, nanostructured materials, nano-particles, carbon nanotubes; additional physical effects – hot charge carriers, generation of several electron-hole pairs by one photon, optical excitation using impurity energy levels; as well as multi-junction structures – tandem, cascade, *etc*.

One of the promising trends for the development of third-generation photoelectric converters is associated with embedding metal nanoparticles into the construction of solar cells, based, as a rule, on amorphous silicon. Although amorphous silicon has a higher solar radiation absorption coefficient than crystalline silicon, the high density of defects serving as recombination centers for electrons and holes limits the diffusion length of minority charge carriers to values not exceeding 100 nm. Therefore, solar cells based on amorphous silicon are made in the form of thin films, the thickness of which does not allow to provide sufficient absorption of solar radiation and to achieve efficiency values above 11-12% [2].

The increase in efficiency of amorphous silicon thin-film solar cells with metal nanoparticles is taking place due to the more efficient retention of photons in the active semiconductor layer. It occurs because of sunlight reflection from nanoparticles into the photoactive layer at different angles and thereby increasing the optical path of photons. The second mechanism for increasing the efficiency is the appearance of surface plasmons – collective oscillations of free electrons on the surface of nanoparticles when radiation interacts with nanoparticles of certain metals [3, 4]. The effect of local surface plasmon resonance appears as the enhancement of the electromagnetic field near the nanoparticles, which leads to an increase in light absorption by the semiconductor material and to a respective increase in the efficiency of the solar cell. In [5], it is noted that metal nanoparticle embedding into the photoactive layer of an amorphous silicon solar cell and surface texturing makes it possible to increase the efficiency by more than 30%.

Metals that support the appearance of surface plasmons are gold (Au), silver (Ag), aluminum (Al) and copper (Cu). Nanoparticles from these metals allow increasing the absorption of optical radiation in thin-film solar cells using both the scattering of light by nanoparticles and the concentration of radiation near the surface of nanoparticles due to plasmon resonance. The contribution of these mechanisms to increasing the efficiency of solar cells is unequal and highly dependent on the location, size, shape, distance between nanoparticles and many other factors.

Most researchers use gold or silver as a material for nanoparticles [6-10]. However, the utilization of noble metals significantly increases the cost of solar modules. At the same time, a metal such as aluminum, which also has the property of maintaining plasmon resonance, can serve as a cheaper replacement for expensive materials. The high efficiency of the solar cell with aluminum nanoparticles located on the illuminated semiconductor surface is shown in [11]. A solar cell with hemispherical aluminum nanoparticles on the surface of a silver reflector and the front surface of an amorphous silicon layer textured with corresponding by shape and size texture elements is studied in [12]. It is noted that the frequency of plasmon resonance for aluminum nanoparticles mainly corresponds to the ultraviolet part of the spectrum, which distinguishes aluminum nanoparticles from those made of noble metals, for which plasmon resonance is observed in the visible part of the spectrum. However, selecting the shape, size of aluminum nanoparticles, as well as other parameters, one can extend the range of resonant frequencies to the visible part of the spectrum. Thus, the use of cheap aluminum nanoparticles is more than justified, and researches devoted to the study of the properties of modern thin-film solar cells coated with aluminum nanoparticles are of great interest.

This article aims to simulate an amorphous silicon thin-film solar cell with aluminum nanoparticles that are placed above the transparent top electrode, as well as between the transparent back electrode and the reflecting screen. Based on the calculation of the intensity of solar radiation in the photoactive layer of amorphous silicon, it is required to obtain and analyze the distribution of photogeneration rate for various sizes of nanoparticles and to determine the electrical characteristics of the solar cell. The simulation results should show that the double-sided coating of a solar cell by nanoparticles electrically isolated from the semiconductor material makes it possible to better retain solar radiation in the photoactive layer and significantly increase the efficiency of the solar cell.

2. Solar cell structure and simulation techniques

Simulation of an amorphous silicon thin-film solar cell with a double-sided arrangement of aluminum nanoparticles above the upper and below the lower transparent electrodes was performed using the Silvaco TCAD software package [13]. The structure of the solar cell is shown in Fig. 1.

The solar cell under consideration is a thin-film p^+-n-n^+ structure, the absorbing layer of which is made of a lightly doped n-type amorphous silicon with the thickness 300 nm. A p-type diffuse layer with the maximum acceptor impurity concentration close to $5\cdot10^{18}$ cm^{-3} and the p-n junction depth of 20 nm is formed at the front side of the absorbing layer. On the back side of the absorbing layer, n-type diffuse layer is formed with the donor concentration 10^{18} cm^{-3} and thickness 30 nm. Transparent indium-tin oxide (ITO) electrodes are deposited onto the front and back sides of the p^+-n-n^+ structure. Aluminum nanoparticles of circular shape insulated from electrodes are placed above the front side electrode and below the back side electrode. The nanoparticles are considered to be placed in layers of a transparent for radiation, lossless material. Under the bottom layer of nanoparticles, a reflecting aluminum screen is located.

The calculation of the radiation intensity required for determining the photogeneration rate, when the structure is irradiated with sunlight, was carried out using

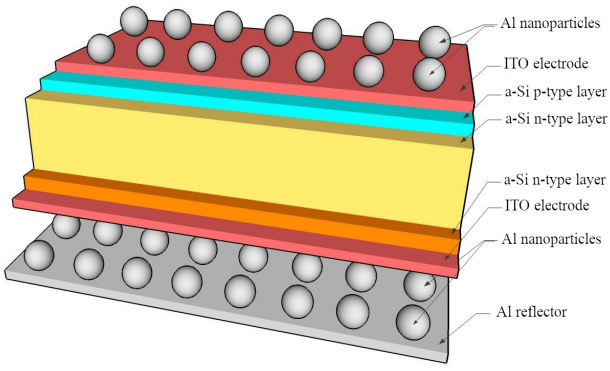

Fig. 1. Solar cell structure.

the FDTD method. Since the structure under consideration is regular along the horizontal direction, periodic boundary conditions were applied at the lateral boundaries of the computational domain. On the upper boundary of the domain from the open space side, the boundary conditions for the perfectly matched layer were used. The incidence of solar radiation on the front surface of the solar cell was modeled by the propagation of a plain cosine-TE wave, which intensity within the wavelength range from 300 up to 800 nm corresponds to the illumination conditions for AM1.5.

The mathematical model used in Silvaco TCAD to analyze the electrical characteristics of semiconductor devices is a system of fundamental equations relating the electrostatic potential and the density of currents for electrons and holes within the area under consideration. These equations include the Poisson equation, continuity equations, and the transport ones.

The Poisson equation relates the electrostatic potential to the space charge density:

$$\mathrm{div}(\varepsilon\nabla\psi) = -\rho\,, \tag{1}$$

where ψ is the electrostatic potential, ε – local dielectric permittivity, ρ – local space charge density. The electric field is defined as the gradient of the potential

$$\vec{E} = -\nabla\psi\,. \tag{2}$$

The continuity equations for electrons and holes are given by the following relations:

$$\begin{aligned} \frac{\partial n}{\partial t} &= \frac{1}{q}\mathrm{div}\vec{J}_n + G_n - R_n\,, \\ \frac{\partial p}{\partial t} &= -\frac{1}{q}\mathrm{div}\vec{J}_p + G_p - R_p\,, \end{aligned} \tag{3}$$

where n and p are the concentrations of electrons and holes, respectively, $\vec{J}_n$ and $\vec{J}_p$ – densities of the electron and hole currents, G_n and G_p – generation rates for electrons and holes, R_n and R_p – recombination rates for electrons and holes, q is the electron charge magnitude.

The type of transport equations determining the values of the electron and hole current densities depends on the chosen transport model – drift-diffusion, energy balance, or hydrodynamic. In this study, the drift-diffusion model is applied, according to which the transport equations are formulated as:

$$\begin{aligned} \vec{J}_n &= qn\mu_n\vec{E}_n + qD_n\nabla n, \\ \vec{J}_p &= qp\mu_p\vec{E}_p - qD_p\nabla p, \end{aligned} \tag{4}$$

where μ_n and μ_p are electron and hole mobilities dependent on carrier concentration, $\vec{E}_n$ and $\vec{E}_p$ – effective electric fields for electrons and holes, D_n and D_p – diffusion coefficients of electrons and holes.

The recombination processes are described in the framework of the Shockley–Read–Hall and Auger recombination models.

Differential equations were discretized in the region occupied by the semiconductor structure using the finite-difference method. The coupled systems of algebraic equations obtained in this way were solved by the iterative Newton method.

3. Numerical results and discussion

The calculation of solar radiation intensity by the FDTD method using the Silvaco TCAD software package allows us to find the values of the photogeneration rate, which directly affects the electrical characteristics of the solar cell. The photogeneration rate in the photoactive layer of the solar cell was calculated for different values of the nanoparticle radius R with a fixed distance between the nanoparticles S, which is equal to 200 nm. The distribution of photogeneration rate in the photoactive layer of amorphous silicon is shown in Fig. 2 for several values of the nanoparticle radius.

The figures demonstrate the appearance of the photogeneration rate maxima and minima with increasing nanoparticle radius. As can be seen from Fig. 2a, nanoparticles with a radius of 1…10 nm have practically no effect on the photogeneration rate distribution in the amorphous silicon layer. As the radius increases to 15…30 nm, the photogeneration rate maxima are observed under the nanoparticles of the front surface and over the nanoparticles of the solar cell back surface. With a further increase in the radius of the nanoparticles, the maxima of photogeneration rate begin to predominantly concentrate under the nanoparticles of the front surface. For nanoparticles with the radius values up to 140 nm, the greatest photogeneration rate is observed in the areas under the nanoparticles of the front surface. With the further increase in the radius, shaded areas are formed under the nanoparticles of the front surface, where the decrease of photogeneration rate is observed. The highest values of photogeneration rate can be reached for a nanoparticle radius close to 25 nm, when the photogeneration rate maxima occur both under the nanoparticles of the front surface and over the nanoparticles of the solar cell back surface.

The distributions of the photogeneration rate along vertical cutlines under the nanoparticles of the front surface and over the nanoparticles of the back surface are shown in Figs. 3 and 4 for nanoparticles of different radii. The distance between the nanoparticles for all values of the radius remains unchanged, being equal to 200 nm.

From the plots in Figs. 3 and 4, it can be seen that, for nanoparticles with the radius 1 nm, the curves of photogeneration rate under the nanoparticles of the front surface and over the nanoparticles of the back surface almost coincide. Thus, nanoparticles of this size do not affect the characteristics of the solar cell. The best photogeneration rates correspond to nanoparticles with the radius close to 25 nm. With the further increase in the

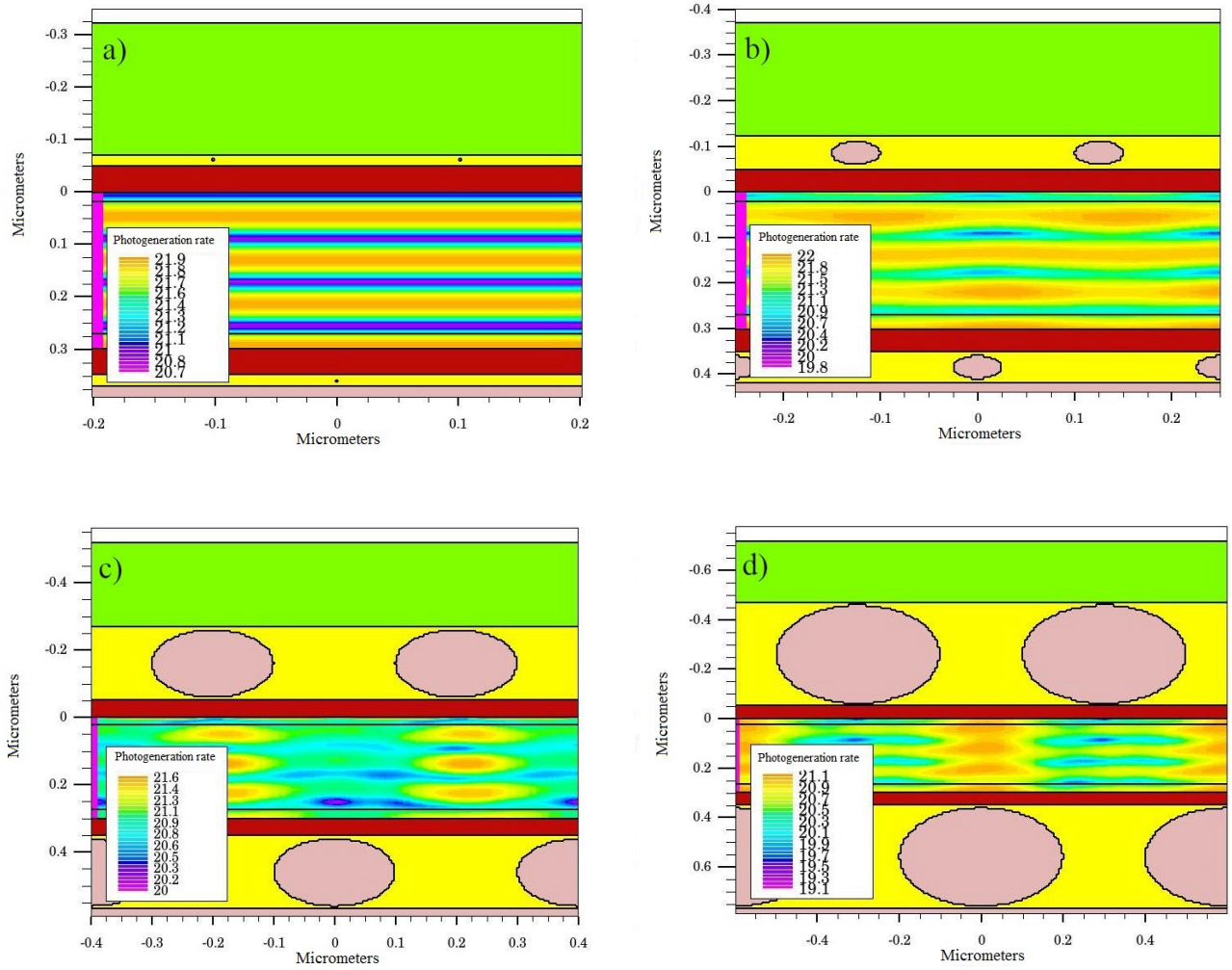

Fig. 2. Photogeneration rate distribution in the layer of amorphous silicon at various nanoparticle radii *R*: 1 (*a*), 25 (*b*), 100 (*c*), 200 nm (*d*).

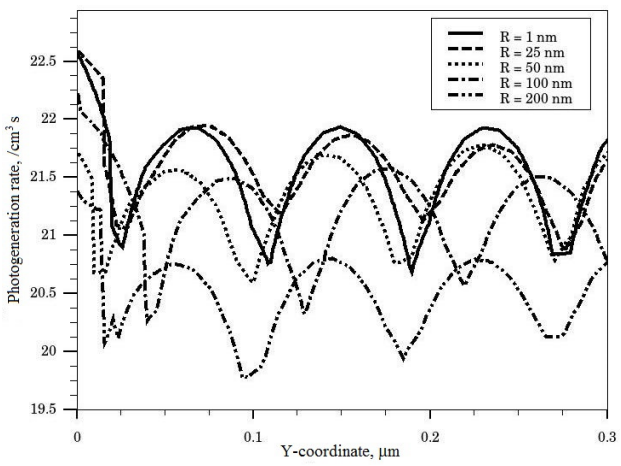

Fig. 3. Photogeneration rate distribution under the nanoparticles of the front surface.

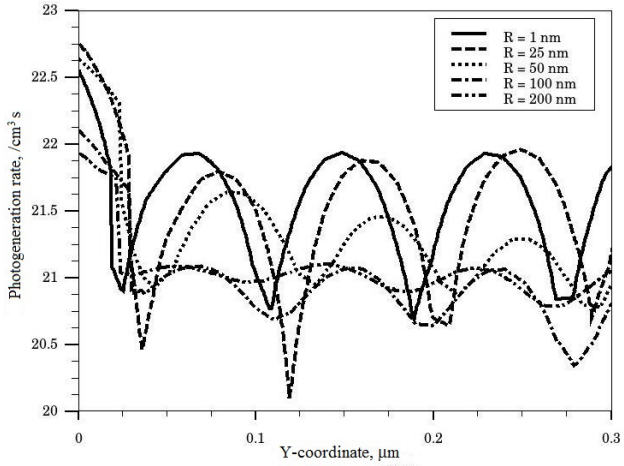

Fig. 4. Photogeneration rate distribution over the nanoparticles of the back surface.

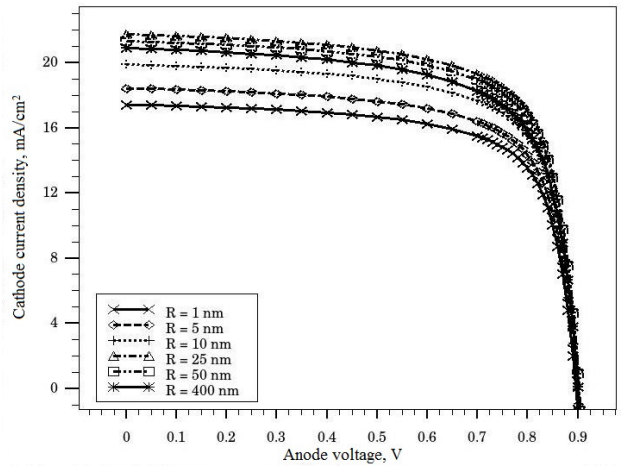

Fig. 5. *I-V* characteristics for various radii of nanoparticles at the fixed interval 200 nm.

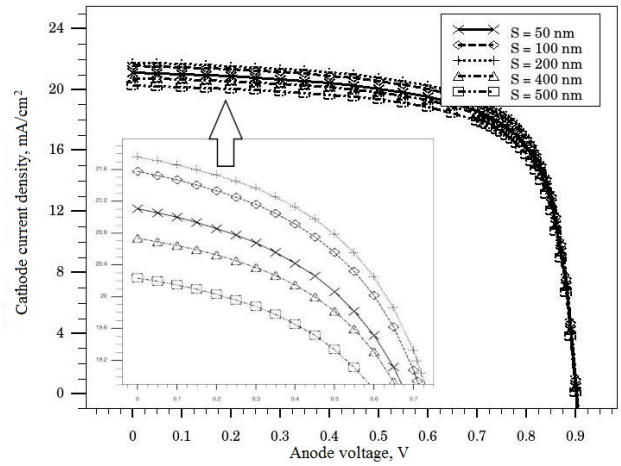

Fig. 6. *I-V* characteristics for various spacings between the nanoparticles at the fixed radius 25 nm.

nanoparticle radius, the photogeneration rate begins to decrease. After formation of shaded areas under the front surface nanoparticles, the photogeneration rate under those nanoparticles begins to decrease rapidly, while over the nanoparticles of the back surface it remains almost unchanged. The current-voltage characteristics of the solar cell, reflecting the dependence of the cathode current on the voltage at the anode, were calculated for different nanoparticle radii and the fixed distance between nanoparticles 200 nm, as well as for different nanoparticle distances for the constant nanoparticle radius 25 nm. The plots of corresponding *I-V* characteristics for cathode current density are shown in Figs. 5 and 6.

The set of curves for the dependence of the cathode current density on the voltage at the anode at a fixed distance between the nanoparticles in Fig. 5 shows that

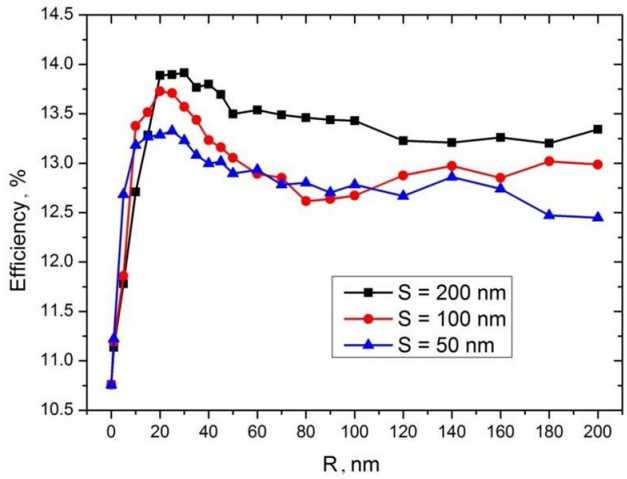

Fig. 7. The dependence of solar cell efficiency on the radius of nanoparticles.

an increase in the nanoparticle radius from 1 up to 25 nm leads to a rapid increase in the cathode current density, which can be associated with the appearance of local maxima of the photogeneration rate. The further increase in the radius contributes to the appearance of shaded areas under the nanoparticles, which leads to the decrease in the cathode current density. As can be seen in Fig. 6, the change in the distance between nanoparticles for a fixed nanoparticle radius also affects the magnitude of the cathode current density. For the specified radius of the nanoparticles, the highest value of the cathode current density can be achieved, when the distance between the nanoparticles is 200 nm.

The most important characteristic of a solar cell is its efficiency. The change in the efficiency of a solar cell with increasing nanoparticle radius is shown in Fig. 7 for different variants of the distance between nanoparticles.

As can be seen from the behavior of the curves, it is possible to achieve a maximum value of efficiency of 13.8% for nanoparticles with the radius 25 nm and with the distance between them 200 nm.

4. Conclusions

The results of computer simulation carried out using the Silvaco TCAD software package showed that the double-sided arrangement of nanoparticles both above the top transparent electrode and below the bottom transparent electrode of the thin-film solar cell contributes to creation of local maxima of the photogeneration rate in the photo-active semiconductor layer, leading to an increase in the photocurrent. The choice of the optimal radius of nano-particles and the distance between these nanoparticles makes it possible to achieve the efficiency up to 13.8% in a thin-film amorphous silicon solar cell. Thus, this design of a solar cell allows us to effectively retain solar radiation in a thin absorbing layer of amorphous silicon by using cheap aluminum as a material for nanoparticles.

References

1. Fthenakis V. (ed.). *Third Generation Photovoltaics.* InTech, Rijeka, Croatia, 2012.
2. Green M.A., Emery K., Hishikawa Y. and Warta W. Solar cell efficiency tables. *Progress in Photovoltaics: Research and Applications.* 2011. **19**. P. 84–92. https://doi.org/10.1002/pip.1088.
3. Atwater H.A. and Polman A. Plasmonics for improved photovoltaic devices. *Nature Material.* 2010. **9**. P. 205–213. https://doi.org/10.1038/ nmat2629.
4. Ferry V.E., Munday J.N. and Atwater H.A. Design considerations for plasmonic photovoltaics. *Adv. Mater.* 2010. **22**. P. 4794–4808. https://doi.org/10.1002/adma.201000488.
5. Ghahremani A. and Fathy A.E. High efficiency thin-film amorphous silicon solar cells. *Energy Sci. and Eng*. 2016. **4**. P. 334–343. https://doi.org/10.1002/ese3.131.
6. Derkacs D., Lim S.H., Matheu P., Mar W. and Yu E.T. Improved performance of amorphous silicon solar cells via scattering from surface plasmon polaritons in nearby metallic nanoparticles. *Appl. Phys. Lett.* 2006. **89**. P. 093103-1–093103-3. https://doi.org/10.1063/1.2336629.
7. Singh Y.P., Kumar A., Jain A. and Kapoor A. Enhancement in optical absorption of plasmonic solar cells. *The Open Renewable Energy Journal*. 2013. **6**. P. 1–6. https://doi.org/10.2174/ 1876387101306010001.
8. Wang P.H., Theuring M., Vehse M., Steenhoff V., Agert C. and Brolo A.G. Light trapping in a-Si:H thin film solar cells using silver nanostructures. *AIP Adv.* 2017. **7**. P. 015019-1–015019-8. https://doi.org//10.1063/1.4973987.
9. Faraone G., Modi R., Marom S., Podest A. and Vece M. Increasing the optical absorption in a-Si thin films by embedding gold nanoparticles. *Optical Materials*. 2018. 75. P. 204–210. https://doi.org/10.1016/j.optmat.2017.10.025.
10. Gandhi K.K., Nejim A., Beliatis M., Mills C.A., Henley S.J. and Silva S.R.P. Simultaneous optical and electrical modeling of plasmonic light trapping in thin-film amorphous silicon photovoltaic devices. *SPIE Journal of Photonics for Energy*. 2015. **5**, No 1. P. 1–22. https://doi.org/10.1117/1.JPE.5.057007.
11. Zhang Y., Cai B. and Jia B. Ultraviolet plasmonic aluminum nanoparticles for highly efficient light incoupling on silicon solar cells. *Nanomaterials.* 2016. **95**, No 6. P. 1–10. https://doi.org/10.3390/nano6060095.
12. Ferry V.E., Polman A. and Atwater H.A. Modeling light trapping in nanostructured solar cells. *ACS Nano*. 2011. **5**, No 12. P. 10055–10064. https://doi.org//10.1021/nn203906t.
13. *ATLAS User's Manual*. Silvaco, Santa Clara, CA, 2015.

Authors and CV

Gnilenko Alexey Borisovich, Ph.D. degree in physics and mathematics, Associate Professor of the Faculty of Physics, Electronics and Computer Systems at the Oles Honchar Dnipro National University, Senior Researcher at the Institute of Transport Systems and Technology, National Academy of Science of Ukraine. His research areas are computational methods in electromagnetics and electronics, computer simulation and design of microwave and semiconductor devises.

Plaksin Sergey Victorovich, Doctor of sciences on physics and mathematics, Senior Researcher, Academician of Transport Academy of Ukraine. Head of the Department of control systems at the Institute of the Transport systems and technologies «Transmag», NAS of Ukraine (Dnipro). He is the author of more than 300 advanced studies, including 6 monographs, 57 patents of Ukraine and 4 author's certificates of USSR, as well as 5 handbooks on semiconductor microwave electronics. His main research is the analysis of parameters of semiconductor materials by microwave methods, photoelectric conversion of solar energy.